Femtosecond second-harmonic generation in periodically poled lithium niobate waveguides with simultaneous strong pump depletion and group-velocity walk-off

Zheng Zheng* and Andrew M. Weiner

School of Electrical and Computer Engineering, Purdue University, 1285 EE Building, West Lafayette, Indiana 47907-1285

Krishnan R. Parameswaran, Ming-Hsien Chou,† and Martin M. Fejer

E. L. Ginzton Laboratory, Stanford University, Stanford, California 94305-4085

Received May 15, 2001; revised manuscript received August 1, 2001

We report studies of second-harmonic generation (SHG) of femtosecond pulses in long periodically poled lithium niobate waveguides under large conversion conditions. Strong saturation of the SHG efficiency was observed, accompanied by spectral and temporal distortion of the pump pulse. Our simulation studies suggest that the pulse distortions may be caused by the interaction of the phase-matched SHG process and an additional cascaded $\chi^{(2)}$ process or processes, leading to a large nonlinear phase modulation. Such additional cascaded $\chi^{(2)}$ processes could be caused by the existence of multiple transverse modes in the nonlinear waveguide. These phenomena, which to our knowledge have not been reported previously, may have a significant effect on studies of high-power short-pulse parametric process in waveguide devices and on the design of novel nonlinear optical waveguide devices for such applications.

OCIS codes: 190.2620, 190.4390, 190.7110, 230.4320.

1. INTRODUCTION

Second-harmonic generation (SHG), first studied in the early 1960s, is among the best-known nonlinear optical phenomena. Investigations of SHG in response to ultrafast optical pulses were also reported in the 1960s.[1,2] These early investigations revealed the importance of group-velocity mismatch (GVM) between the fundamental and the second-harmonic waves when the GVM is sufficiently large compared with the pulse duration, the GVM leads to a broadening of the generated second-harmonic pulse with respect to the input pulse, together with a narrowing of the phase-matching bandwidth. To avoid these usually unwanted effects, femtosecond SHG experiments normally use short nonlinear crystals with a small GVM. However, we recently used thick nonlinear crystals with a large GVM to perform several femtosecond SHG experiments. Our results demonstrate several interesting and unique features. These include the possibility of high conversion efficiency at low input power,[3] especially when waveguide devices are used,[4] at the cost of the second-harmonic pulse width, and also include all-optical signal processing for high-contrast ultrafast waveform recognition.[4,5] Here we present detailed experimental data on femtosecond SHG in periodically poled lithium niobate (PPLN) waveguides under conditions of simultaneous strong pump depletion and large GVM. This parameter regime has seen very little, if any, previous experimental investigation.

Nonlinear devices based on quasi-phase-matched (QPM) materials such as PPLN[6–8] can provide relatively large nonlinearities while opening up additional degrees of freedom for engineering the nonlinear output.[9–11] For example, nonlinear crystals with chirped and patterned QPM gratings have been used for pulse compression and pulse shaping in femtosecond SHG.[9,10] Nonlinear optical waveguides promise even greater nonlinear efficiencies owing to their confined optical fields and long interaction lengths. However, additional complexities arise in designing waveguide nonlinear devices. Issues related to control and optimization of interacting spatial modes have a significant effect on device behavior.[12,13] Usually waveguide design efforts focus on the pair of modes at fundamental and second-harmonic wavelengths that give the best mode overlap and thus the highest efficiency for frequency conversion. Although in most cases other spatial modes exist, their effect on nonlinear device performance is often neglected.

Here we present the results of experimental and theoretical studies of femtosecond pulse SHG in long PPLN waveguides under the high pump depletion condition. Although a SHG conversion efficiency of ~60% is easily obtained at input energies of only a few picojoules, we observed a surprisingly strong saturation that prevented the efficiency from increasing significantly above this value. We also observed a strong reshaping of the temporal and spectral profiles of the input pulse that is not

0740-3224/2002/040839-10$15.00

expected under the standard two-coupled-wave treatment of SHG. Our theoretical simulation studies suggest that an additional, very large nonlinear phase modulation process may be responsible for these effects. Although the origin of this phase modulation is not yet pinned down, we believe that new channels for cascaded $\chi^{(2)}$ processes involving multiple spatial waveguide modes may be responsible.

High depletion of ultrashort pulses through SHG may find potential applications in wavelength conversion, short-wavelength generation, generation of amplitude-squeezed light,[14] and all-optical signal processing in optical communication systems. For example, an optical add–drop multiplexer for ultrashort pulse code-division multiple-access optical communications[15] could be realized by the scheme illustrated in Fig. 1. The function of the add–drop multiplexer is to selectively drop a channel represented by a specific optical waveform (or code) from the main data stream in the network without affecting other transmitted channels represented by other distinct waveforms (codes). We previously demonstrated that SHG in a long nonlinear crystal with large GVM can function as a spectral phase correlator, which provides a strong contrast (approaching 30 dB) in the SHG yield between certain properly and improperly coded waveforms.[5,4] Therefore a channel dropper could be constructed with two pulse shapers and a long SHG crystal, as shown in Fig. 1. After the first pulse shaper performs a decoding operation, the SHG process preferentially converts waveforms with the selected code into the second harmonic, which can then be separated from the remaining data by a wavelength demultiplexer. The second pulse shaper performs the operation inverse to that of the first pulse shaper, so that the output waveforms in the remaining channels are the same as at the input. Note that complete dropping of the selected channel would require nearly 100% conversion of the appropriate optical pulses to the second-harmonic wavelength, which has not been achieved in our studies so far. This provides a motivation for the research presented in this paper, in which we seek to gain insight into the processes limiting the achievement of 100% conversion in the large GVM regime.

In this paper we first present our experimental results on SHG of femtosecond pulses in a long PPLN waveguide at a 1.56-μm wavelength under high-depletion conditions. We observe strong saturation of the SHG conversion efficiency accompanied by temporal breakup of the 1.56-μm pump pulse and distortion of its power spectrum, which cannot be explained by the SHG process alone. We then present theoretical studies in which we solve the coupled propagation equations numerically. By assuming a negative nonlinear phase modulation process approximately 2 orders of magnitude stronger than the normal optical Kerr effect, we are able to simulate the experimental results. Finally, we discuss simulation results supporting the possibility that this nonlinear phase distortion arises from a cascaded $\chi^{(2)}$ process that may involve additional non-phase-matched waveguide modes.

2. EXPERIMENTAL STUDIES

In our experimental setup, the fundamental light came from a Spectra-Physics femtosecond optical parametric oscillator synchronously pumped by a mode-locked Ti:sapphire laser. The pulses were nearly transform limited and had a width of ~200–250 fs. The spectral FWHM bandwidth was ~12 nm, and the center wavelength was tunable around 1560 nm. The beam was focused into the PPLN waveguide by free-space coupling.

Our PPLN sample[4] included a 55.5-mm-long SHG section with a 12-μm waveguide width and with a nominally uniform grating period of 14.75 μm. The 12-μm waveguide width was chosen to achieve noncritical QPM, so that the phase-matching frequency became relatively insensitive to small errors in the waveguide dimensions.[12] The input and output ends of the sample incorporated 4-μm-wide mode-filter sections, which were linearly tapered over a several-millimeter distance to the 12-μm width of the SHG region. Since the SHG section supports multiple transverse modes at both the pump and the SHG wavelengths, the mode filter facilitates coupling into the fundamental transverse mode of the waveguide by suppressing higher-order spatial modes at the pump wavelength.[16] Waveguide fabrication was performed by proton exchange to a depth of 0.71 μm followed by annealing for 26 h at 328 °C in air. The phase-matching condition was temperature tuned, and, for a 1560-nm input, the phase-matching temperature was ~100 °C. The GVM of the annealed proton exchanged waveguide is ~0.37 ps/mm, corresponding to a total GVM of ~20.5 ps. This implies a theoretical second-harmonic phase-matching bandwidth of ~0.1 nm.

We measured the SHG efficiency as a function of input pump power, with the phase-matching wavelength of the PPLN sample set for phase matching of an ~779-nm second-harmonic wavelength (~1558 center wavelength for the fundamental). As is shown in Fig. 2, we can see an ~50%/pJ small-signal SHG efficiency for pump pulse energies below 1 pJ, similar to what was observed in Ref. 4. However, the SHG efficiency quickly saturates at ~60% at pulse energy levels above 2 pJ. Also plotted in the figure is the theoretical curve, calculated assuming an ideal SHG process under the large GVM condition. The calculation procedure is described in greater detail in Section 3. It is obvious that the experimental efficiency saturates considerably more strongly than does the theorical.

We note that, under high depletion conditions (several-picojoule pump energy), we also observed some weak

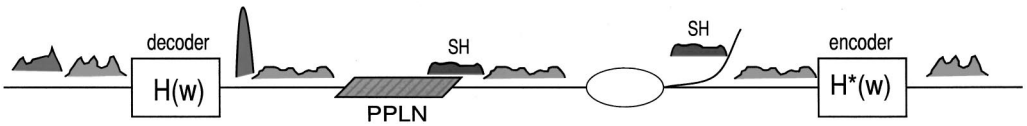

Fig. 1. Scheme of proposed add–drop multiplexer for code-division multiple-access systems. SH, second harmonic.

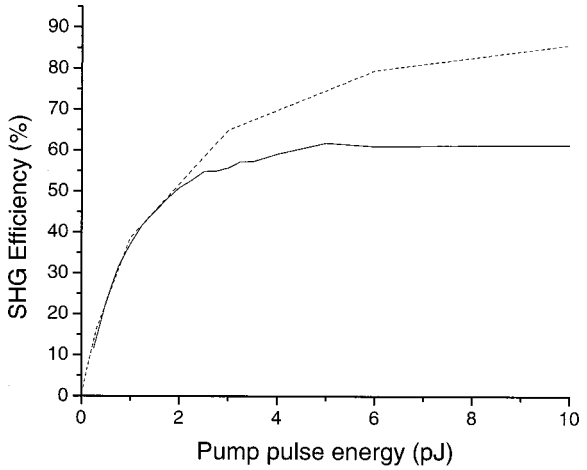

Fig. 2. SHG efficiency versus pump pulse energy. Solid curve, experimental result; Dashed curve, theoretical result.

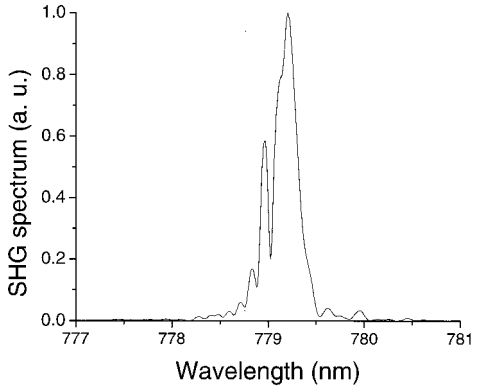

Fig. 3. Second-harmonic spectrum shape under low-power pump conditions.

green light generated from the sample, which we attribute to sum-frequency mixing of the fundamental and the second harmonic waves through a nearly phase-matched third-order QPM process.[17] We also measured the output pump power and the second-harmonic power individually as a function of input pump powers up to 10 pJ. The ratio of the total output power to the input power remained constant to within our experimental accuracy of ~10%. This shows that nonlinear loss mechanisms do not play a significant role in our experiments.

To gain insight into the surprising saturation behavior, we performed a series of additional measurements. First, we measured the SHG spectrum by using an optical spectrum analyzer, which had a spectral resolution of ~0.08 nm. As is seen in Fig. 3, at low input powers the SHG spectrum had a FWHM bandwidth of ~0.3 nm with a long oscillating tail on the short-wavelength side. The deviation from the ideal sinc^2 shape may be caused by inhomogeneities in the device structure or a nonuniform temperature distribution in the PPLN oven.[18] We address this issue in Section 3.

Second, the temporal profile of the transmitted pump pulse at 1560 nm was measured by means of electric field cross correlation. The reference pulse was taken directly from the output of the optical parametric oscillator. The data are shown in Fig. 4. At low input power the width of the trace is ~250 fs, which is close to that estimated from the inverse spectral bandwidth. This indicates that there is no significant pulse broadening or distortion at low power; accordingly, we conclude that the effect of group-velocity dispersion (GVD) on the propagation of the fundamental pulse is small in our waveguide device. On the other hand, at high input levels (>2 pJ) the pump pulse begins to change significantly. At an ~10-pJ input, a double-hump pulse shape was observed, as shown in Fig. 4(b).

We also repeated the cross-correlation measurements with the phase-matching wavelength detuned to ~774 nm (~1548 nm at the fundamental). As a result, the SHG output was reduced by more than 1 order of magnitude compared with the phase-matched cases discussed above. For both low- and high-power inputs, the observed cross-correlation traces, shown in Fig. 5, are essentially identical to the low-power trace shown in Fig. 4(a). Furthermore, the distortion evident at high power in the phase-matched case, Fig. 4(b), is no longer observed. This indicates that the pulse distortion is linked to the parametric process(es) and does not arise solely from processes such as the optical Kerr effect (e.g., self-phase modulation, SPM).

The spectra of the pump pulses exiting the SHG sample were also measured under similar conditions with an op-

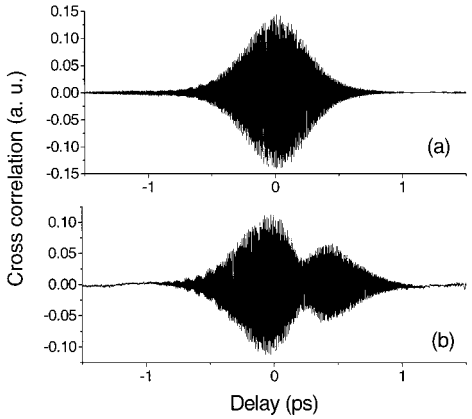

Fig. 4. Pump pulse temporal shape when it is phase matched for SHG (a) at 0.5-pJ power level, (b) at 10-pJ power level.

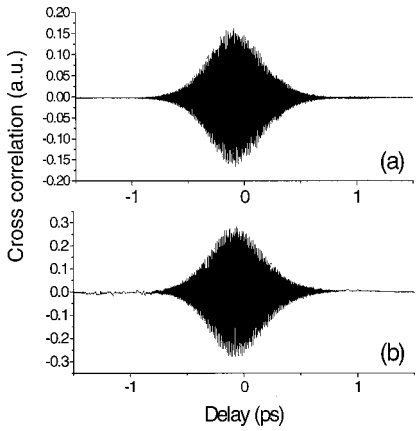

Fig. 5. Pump pulse temporal shape when it is not phase matched for SHG (a) at 0.5-pJ power level, (b) at 10-pJ power level.

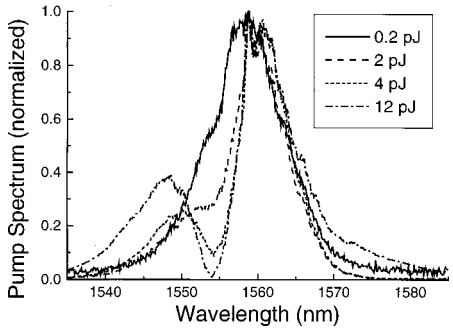

Fig. 6. Pump spectrum variation as the pump power increases.

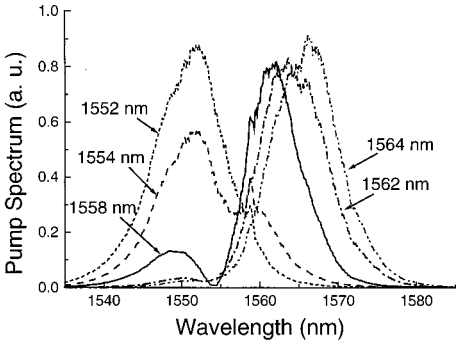

Fig. 7. Output pump spectrum under high-power conditions. The center wavelength is varied while the phase-matching wavelength of the sample is fixed at ~1558 nm. The labels show the center wavelengths of the input pump spectrum.

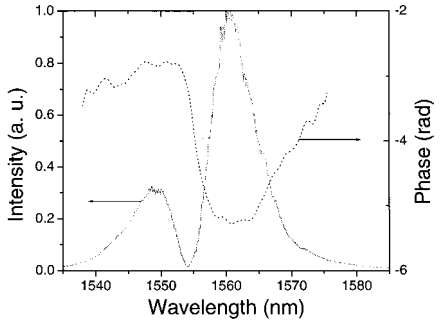

Fig. 8. Spectral phase curve of the pump under the phase-matched and high-power input condition. Measured at ~10 pJ power level.

tical spectrum analyzer (see Fig. 6). For these measurements the phase-matching wavelength was set to ~1558.5 nm. When the SHG efficiency is low, the output pump spectrum has a shape similar to that of the input pump spectrum, which indicates a uniform depletion of the pump spectral components. As the pump power increases, the pump spectrum becomes asymmetric, even though the phase-matching wavelength is at the center of the pump spectrum. The shorter-wavelength side is significantly suppressed, and a pronounced spectral dip forms around 1554 nm when the pump power is close to 10 pJ, which coincides with the occurrence of the double-hump temporal shape discussed above. Simultaneously, some spectral broadening was also observed in both the short- and the long-wavelength tails of the spectrum. We also measured the pump output spectra for a fixed ~1558.5-nm phase-matching wavelength and 10-pJ input pump energy while tuning the input pump wavelength. As is shown in Fig. 7, the results show significant but asymmetric distortions at this energy level as long as the phase-matching wavelength is within the FWHM of the pump spectrum.

Besides the spectral intensity distributions, we further analyzed the pump signal by performing spectral interferometry[19] measurements to retrieve the spectral phase information. When the pump spectrum is centered at the phase-matching wavelength, ~1558.5 nm, a significant phase jump centered at the spectral amplitude dip begins to emerge as the pump power increases. As is shown in Fig. 8, the phase variation exceeds 2 rad at a 10-pJ input energy level. The measurements performed under low-power conditions showed no sign of such a phase variation.

Summarizing this section, our experiments reveal a surprisingly strong saturation of the SHG efficiency accompanied by a significant nonlinear distortion of the pump pulses. Our experimental results also seem to exclude simple effects, such as GVD or SPM arising from the optical Kerr effect, as the origin of these phenomena. An explanation may lie in a more complicated interaction of several nonlinear optical processes. We explore this problem theoretically in the following section through simulations.

3. THEORETICAL AND NUMERICAL STUDIES

Based on the plane wave and slowly varying envelope approximations, the following coupled partial differential equations can be used to describe the evolution of the fundamental and the second-harmonic pulses:

$$\frac{\partial A_1}{\partial z} + \left(\frac{1}{v_{g,1}} - \frac{1}{v_{g,2}}\right)\frac{\partial A_1}{\partial \tau} - \frac{j}{2}\beta_{2,1}\frac{\partial^2 A_1}{\partial \tau^2} = -j\gamma d(z) A_2 A_1^* \exp[-j\Delta k_0(z) z] - j\frac{n_2 k_{1,0}}{n_0}(|A_1|^2 + 2|A_2|^2)A_1 - \frac{\alpha_1}{2}A_1, \quad (1)$$

$$\frac{\partial A_2}{\partial z} - \frac{j}{2}\beta_{2,2}\frac{\partial^2 A_2}{\partial \tau^2} = -j\gamma d(z) A_1^2 \exp[j\Delta k_0(z) z] - j\frac{n_2 k_{2,0}}{n_0}(|A_2|^2 + 2|A_1|^2)A_2 - \frac{\alpha_2}{2}A_2, \quad (2)$$

where A_i is the envelope function of the electric field and $v_{g,i}$ is the group velocity. Here the indices 1 and 2 represent the pump and the second harmonic, respectively; α_i is the linear loss of the material, $\beta_{2,i}$ is the GVD parameter, γ is the SHG coupling coefficient, n_2 is the third-order nonlinear refractive index, and n_0 is the refractive

index. For $LiNbO_3$, we take $n_0 = 2.14$; n_2 is of the order of 10×10^{-16} cm^2/W for bulk lithium niobate,[20] and the resulting maximum nonlinear phase shift for a 10-pJ pump pulse energy should be less than 0.1 rad. We ignore the variation in these numbers for different wavelengths (this does not affect our results much, as is explained below). Here $\tau = t - z/v_{g,2}$ is used, which corresponds to a frame of reference moving with the second-harmonic pulse at velocity $v_{g,2}$. Δk_0 is the phase mismatch at the center frequencies of the pump and second-harmonic pulses.

The above equations include the effects of GVM, linear loss, SPM (and cross-phase modulation, XPM) and SHG, including pump depletion. Though the GVD characteristics of the waveguide are not readily available, we take $\beta_2 = 100$ ps^2/km based on the estimation from the bulk values at the pump wavelength.[10] For the second-harmonic pulse, the same β_2 number was used. Because of the relatively narrow bandwidth of the second-harmonic signal, the resulting error should be small. For ~200-fs pulses, the dispersion length[21] is several times larger than our sample length. This is also consistent with our experimental observations (see Fig. 5). Thus GVD does not seem to be significant in our experiments. Nevertheless, it is included in the model for completeness.

Because of the GVM, the second-harmonic pulse has a long temporal shape, and its peak power is much lower than that of the pump pulse. Therefore it was found that the XPM terms and the SPM term for the second-harmonic signal affect the outcomes of our simulation significantly less than the SPM term corresponding to the pump signal. Based on the intrinsic material nonlinearity, these $\chi^{(3)}$ effects should be weak within our power range. The key parameters used in the simulation are listed in Table 1.

In periodically poled devices, $d(z)$ is a periodic function of z, and the SHG phase mismatch is nonzero. In our simulation, however, for simplicity we consider only the first-order effect of the QPM structure. For ideal first-order QPM, the SHG material can be considered uniform and perfectly phase matched with an effective nonlinearity $d_{\text{eff}} = 2d/\pi$ (where d is the intrinsic nonlinear susceptibility). This allows us to treat $d(z)$ as a constant throughout the material and to set $\Delta k_0 = 0$. As the interacting pulses have relatively broad bandwidths, the phase mismatch of interactions between different frequency components deviates from Δk_0. In Eqs. (1) and (2), the GVM term takes into account the linear spectral variation of the phase mismatch, though the Δk_0 term itself has no frequency dependence. This is equivalent to the frequency domain equations used in Ref. 11 with no explicit GVM term but a frequency-dependent phase-mismatch term. We note that this is fundamentally different from pure frequency-domain studies of cascaded $\chi^{(2)}$ processes, where the phase mismatch is taken as a constant number. We found that other effects (discussed below in this section) have relatively weak effects on the calculated small-signal SHG efficiency.

Table 1. Simulation Parameters

Parameter	Value
Fundamental mode size	40 μm^2
Second-harmonic mode size	10 μm^2
Overlap area[a]	53.1 μm^2
Crystal length	6 cm
Refractive index	2.14
$1/v_{g,1} - 1/v_{g,2}$	0.37 ps/mm
β_2	100 ps^2/km
α_1	0.35 dB/cm
α_2	0.7 dB/cm
d_{eff}	16.5 pm/V

[a] Refs. 12, 22.

In real devices the local QPM wavelength may vary because of either a nonideal device or nonuniform experimental conditions, such as oven temperature distributions. Any such deviations from uniform QPM can be described by a spatially varying $\Delta k_0(z)$ term. This effect is further discussed below.

Equations (1) and (2) were solved numerically by a symmetrized split-step Fourier method.[11,23,24] The parameters used in the simulation, such as waveguide loss and the GVM parameter, were decided on the basis of either previously published values[4,25] or values near known bulk values within a reasonable range.

We first calculated the SHG efficiency for an input sech(t/T_0) pulse with $T_0 = 140$ fs (corresponds to an intensity profile with a duration of 246 fs FWHM), with the GVD and SPM terms set to zero. The results represent the ideal SHG case under large GVM, shown in Fig. 2. Our experimental results for the efficiency clearly cannot be explained by this simplified picture. A better match to the results, would require more factors to be taken into consideration.

Since our observed SHG spectra show a shape significantly different from a sinc^2 shape, the phase-matching condition may be spatially nonuniform. In our experimental setup, the end surfaces of the crystal in our homemade oven were exposed to open air. Therefore the temperatures at the end surfaces are expected to be lower than at the center part of the oven. At high temperatures this difference could be as large as several degrees. We try to model the temperature distribution by incorporating a varying temperature profile $\Delta T(z)$, which results in a spatial variation[18] of Δk. The temperature profile $\Delta T = \Delta T_1 + \Delta T_2$ is taken as[18]

$$\Delta T_i = \begin{cases} T_{Ni}\left(\dfrac{z_{ui} - z}{z_{Ni}}\right)^{p_i} & z \leqslant z_{ui} \\ 0 & z_{ui} < z \leqslant z_{oi} \\ T_{Ni}\left(\dfrac{z - z_{oi}}{z_{Ni}}\right)^{p_i} & z_{oi} < z \end{cases}. \tag{3}$$

We adjusted the parameters in this equation to try to match the low-power SHG spectrum. For $z_{o1} = 28.75$ mm, $z_{u1} = 26.75$ mm, $z_{N1} = 10$ mm, $p_1 = 4.3$, $T_{N1} = 0.06$, $z_{o2} = 27.75$ mm, $z_{u2} = 27.75$ mm, $z_{N2} = 25$ mm, $p_2 = 1.2$, and $T_{N2} = 0.72$, the simulated SHG spectrum is given in Fig. 9. With these parameters the effective temperature at the ends is ~6 deg lower than at the center. The result shows asymmetric and oscillatory

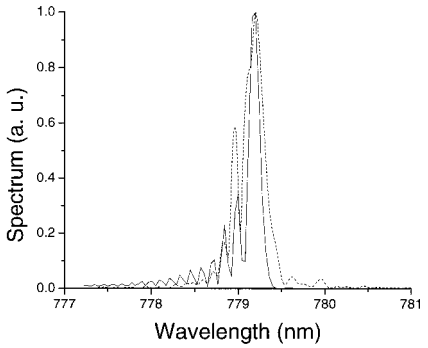

Fig. 9. Simulated and experimental second-harmonic spectrum under low input power. Solid curve, simulation result; Dashed curve, experimental result.

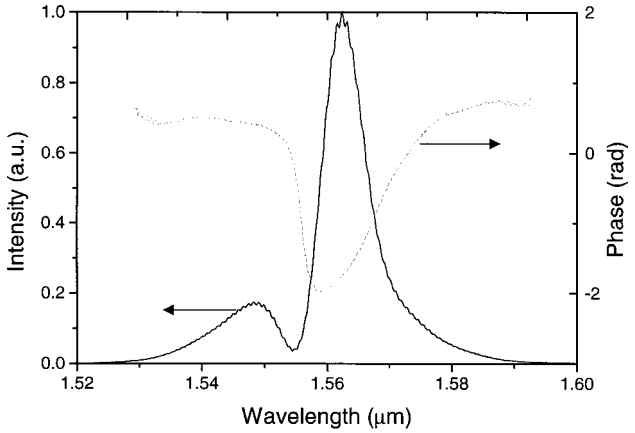

Fig. 10. Simulated pump spectrum under 10 pJ of input power, considering an effective varying phase mismatch and an effective NPM term.

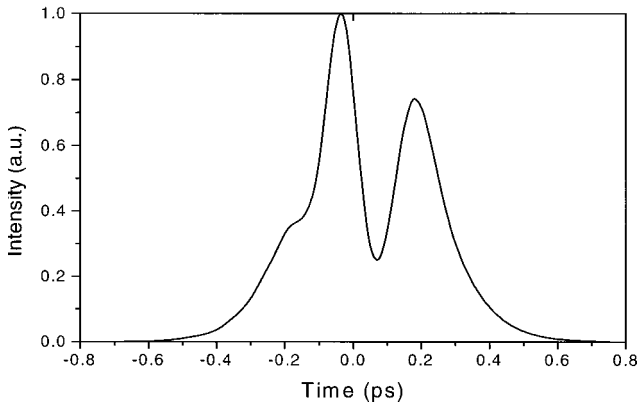

Fig. 11. Simulated pump pulse shape under 10 pJ of input power, considering an effective varying phase mismatch and an effective NPM term.

features similar to the measured result. As is shown in Fig. 12 below, the spatially varying phase mismatch leads to some reduction in the SHG efficiency at high powers but still does not account for the bulk of the saturation. We also found that inclusion of the spatially varying phase mismatch is insufficient to explain our observations of strong temporal and spectral reshaping of the pump pulse.

To reasonably fit the simulation results to the data, we found that it was necessary to include a nonlinear phase-modulation (NPM) term for the pump pulse with a large negative coefficient (approximately -2000×10^{-16} cm^2/W). This term uses the same form as the SPM term in Eq. (1) but with an assumed nonlinear coefficient that is negative and ~2 orders of magnitude larger than the intrinsic n_2. When the large NPM term is included, the calculated pump spectrum shows a short-wavelength dip and a phase jump similar to what we measured in the experiments (see Fig. 10). The simulated temporal intensity profile at a 10-pJ pump power, shown in Fig. 11, is double peaked, again similar to our experimental finding. Such important features are absent in other simulations that include the spatially varying Δk term but only the intrinsic n_2. The simulated SHG efficiency (Fig. 12) also matches the measured results much more closely. The combination of a spatially varying Δk and the NPM term yield a significantly closer match to the experimental results at our highest-power conditions, though it is still difficult to match all the results at all power levels.

We also simulated our experimental studies (see Fig. 7) in which the input center wavelength was detuned from the phase-matching wavelength. A 10-pJ input energy was assumed. Different constant phase mismatches were introduced in the simulation in order to change the relative difference between the input wavelength and the phase-matching wavelength. This is the same as experimentally tuning the input wavelength while keeping the phase-matching wavelength constant. As is shown in Fig. 13, the simulation results are similar to the experimental data. For the cases that correspond to tuning to longer input wavelengths by a few nanometers, there is not much spectral distortion. On the other hand, for tuning to shorter input wavelengths, the simulated results resemble the experimental results qualitatively, although the extension of the simulated spectra on the short-wavelength side is somewhat too large.

The picture so far is as follows. First, the large NPM generates a chirp in the pump pulse. Second, because of the large temporal walk-off, the trailing edge of the pump interacts differently with the second-harmonic signal than does the front edge of the pulse. The observed spectral and temporal distortions arise because of the separation of different pump frequency components in the time

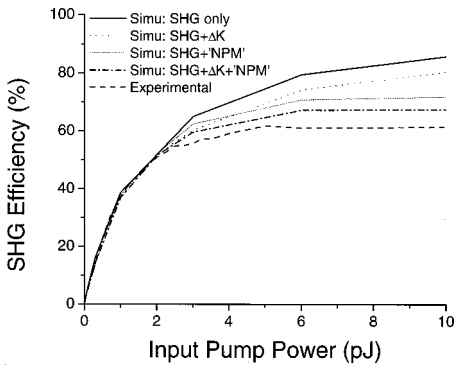

Fig. 12. Simulated (Simu) second-harmonic conversion efficiency versus input pump power, considering the effects of different physical processes.

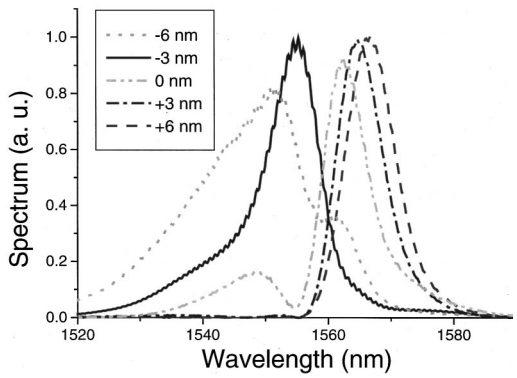

Fig. 13. Simulated pump spectrum under high-power input condition and varied phase-matching conditions. The legend shows the difference between the input pump center wavelength and the phase-matching wavelength.

domain coupled with their interaction with the second-harmonic wave, which also walks off from the pump pulse in time.

Note that for most materials the intrinsic n_2 from the optical Kerr effect is positive and much smaller than what we assumed in our simulation, except in the presence of nonlinear absorptions.[26] In the following we discuss the physical origin of the large negative NPM, which we have included phenomenologically to better match the simulation results with experimental observations.

One possibility that has been discussed is that higher Fourier components of the QPM grating may result in an intensity-dependent phase shift.[27,28] The idea is that considering only the lowest Fourier component of the QPM structure does not give complete results when large growth of the second-harmonic wave occurs within a single QPM period. When significant pump depletion occurs in a single period, as in Ref. 28 for intensities of tens of giga watts per square centimeter and higher in bulk PPLN, the local phase mismatch within a single QPM period must also be considered. At our relatively low pump power levels (<1 GW/cm^2), substantial growth of the second-harmonic wave requires of the order of a few hundred QPM periods. Therefore considering only the lowest Fourier component of the QPM grating should be valid. We conclude, then, that the small, positive phase shift, as described in Ref. 26, cannot explain the large, negative NPM that we are considering here.

The more plausible explanation of the NPM may come from cascaded $\chi^{(2)}$ processes. In a parametric $\chi^{(2)}$ process with nonzero phase mismatch, the conversion and backconversion between the waves can add phase shifts caused by the phase mismatch of the interacting waves. These phase shifts are said to constitute a cascaded $\chi^{(2)}$ process, which has been shown to resemble a $\chi^{(3)}$ process.[29–32] The most common cascaded $\chi^{(2)}$ effects involve a single-step process, such as SHG. Cascade phase shifts in multistep parametric processes, such as third-harmonic generation (THG) arising from SHG followed by sum-frequency generation, have also been discussed.[33–35]

Such cascade phenomena have been intensively studied as substitutes for intrinsic $\chi^{(3)}$ effects for applications like all-optical switching[36] and pulse compression.[37] An important characteristic of the cascaded $\chi^{(2)}$ process is that the magnitude and polarity of the phase shift are related to the phase mismatch of the $\chi^{(2)}$ process. Nonlinear phase shifts, which are very large compared with intrinsic $\chi^{(3)}$ processes, as well as both positive and negative effective n_2,[36] can be realized by controlling the phase-mismatch condition. It has been shown that an effective n_2 as large as $\sim 10 \times 10^{-12}$ cm^2/W can be obtained from SHG processes in PPLN.[36]

Theoretically, Eqs. (1) and (2) already include the possibility of cascaded $\chi^{(2)}$ phase shifts within the main SHG process. The simulations show that any such phase shifts are far too small to explain our experimental observations. However, the additional large NPM may originate from cascade effects in an additional, simultaneous parametric process. Although single cascaded processes have been studied extensively, the interaction between a phase-matched parametric process and an additional cascaded process remains largely unexplored, especially experimentally. Our results here suggest that such effects can have a significant impact on real applications.

The additional cascaded process could come from either another SHG channel, as we describe below, or a multistep process. Experimentally we observed some light from a green generation process. Simultaneous occurrence of more than one QPM $\chi^{(2)}$ process has been observed often in QPM materials.[17,38,39] For PPLN, under our phase-matching condition, a third-order QPM green generation process based on sum-frequency generation can also be nearly phase matched. Such a THG process has been shown in Refs. 33–35 potentially to generate nonlinear phase shifts. Another possibility is an optical parametric amplification process that involves the fundamental pump mode, the generated second-harmonic signal, and another higher-order spatial mode of the pump. As noted above, our $LiNbO_3$ waveguide devices support multiple transverse spatial modes at both the pump and SHG wavelengths. Because different spatial modes have different effective refractive indices, different pairs of fundamental and second-harmonic modes phase match at different wavelengths.[12] Because of the mode filter, only the fundamental spatial mode of the pump is initially seeded; however, higher-order spatial modes at the pump wavelength can be generated through a difference-frequency generation process. We have performed simulations of both the THG and optical parametric amplification multistep processes. At the relatively low power levels investigated here, our simulations suggest that the influence from these processes is relatively weak. For example, in the THG case, the strength of the sum-frequency mixing between fundamental and second harmonic wavelengths must be artificially increased by more than an order of magnitude from the normally acceptable level to yield the nonlinear phase shifts needed to give a small second peak in the pump spectrum at 10 pJ of input energy. Also, the NPM caused by such multistep cascaded processes behaves more like a higher-order nonlinearity[33] than like SPM. As a result, our simulation results based on these multistep models vary much more rapidly with changes in pump power than do our experimental results.

From our simulations with different models, it appears that a cascaded SHG process involving a second (higher-

order) spatial mode of the second harmonic could be the most likely source of the large NPM. For a fixed temperature, the phase-matching wavelengths for either the fundamental or a higher-order second-harmonic mode could be several nanometers to tens of nanometers apart. To model the effect of an additional nearly phase-matched SHG channel, we used a modified set of SHG equations:

$$\frac{\partial A_1}{\partial z} + \left(\frac{1}{v_{g,1}} - \frac{1}{v_{g,2}}\right)\frac{\partial A_1}{\partial \tau} = -j\gamma d A_2 A_1^* \exp(-j\Delta k_0 z) - j\gamma' d A_2' A_1^* \exp(-j\Delta k_0' z) - \frac{\alpha_1}{2} A_1, \quad (4)$$

$$\frac{\partial A_2}{\partial z} = -j\gamma d A_1^2 \times \exp(j\Delta k_0 z) - \frac{\alpha_2}{2} A_2, \quad (5)$$

$$\frac{\partial A_2'}{\partial z} = -j\gamma' d A_1^2 \times \exp(j\Delta k_0' z) - \frac{\alpha_2}{2} A_2', \quad (6)$$

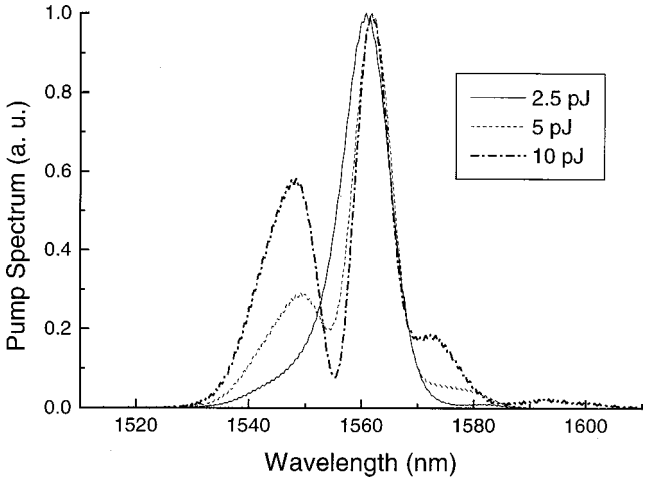

Fig. 14. Simulated pump spectrum under varied pump power conditions considering a second phase-mismatched SHG process.

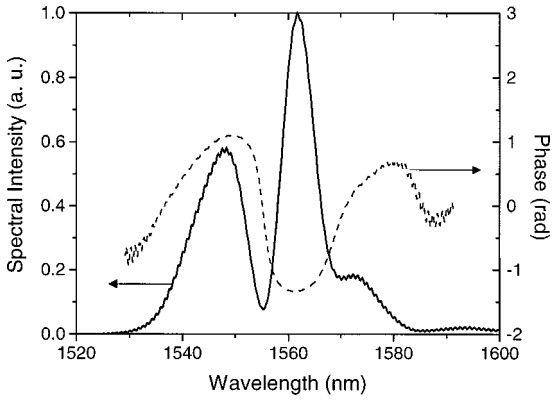

Fig. 15. Simulated pump spectrum and spectral phase curve under a 10-pJ pump power level considering a second phase-mismatched SHG process.

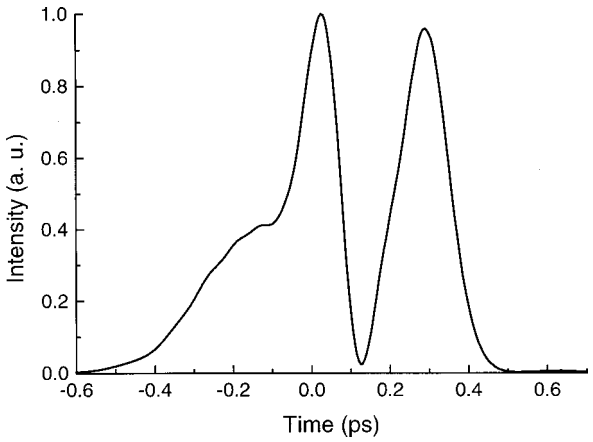

Fig. 16. Simulated pump pulse shape under a 10-pJ pump power level considering a second phase-mismatched SHG process.

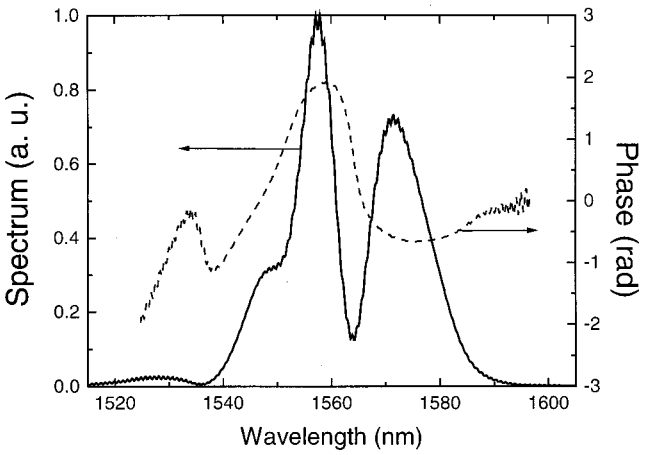

Fig. 17. Simulated pump spectrum and spectral phase curve under a 10-pJ pump power level considering a second phase-mismatched SHG process, assuming a phase mismatch of sign opposite that assumed in Fig. 16.

where Eq. (6) and the terms involving A_2' represent the phase-mismatched SHG channel that could generate the nonlinear phase shift. We assumed that the group velocity and losses of the two second-harmonic signals are the same and set the GVD and $\chi^{(3)}$ SPM and XPM terms to zero. We use the same nonlinear coupling coefficient for the two SHG process ($\gamma = \gamma'$). This ignores the different overlap integrals between the pump mode and the two SHG modes, but this should be sufficient to gain physical insight. The phase-matching wavelength of the second SHG process is taken as 15 nm longer than the center wavelength.

Figure 14 shows the pump spectrum under different pump power levels. The results show the generation of the spectral dip and larger sidelobes at pulse energies above 2.5 pJ. Compared with Fig. 6, the simulation results have strong similarities to the experimental results for comparable power levels. It is noted that the simulated spectral distortions seem to be slightly larger than those experimentally observed. This could indicate that the strength of the cascaded $\chi^{(2)}$ process that we used is somewhat larger than the real one. Shown in Fig. 15 is

the simulation results of the spectral amplitude and phase at a 10-pJ pump energy. The magnitude and shape of the spectral phase jump around the spectral dip also matches that in Fig. 8. In the temporal domain, the breakup of the pump pulse is shown in the simulation in Fig. 16. Thus these results match the experimental results and the earlier simulation results reasonably well and also prove that a cascaded $\chi^{(2)}$ process significantly away from the center, wavelength could generate strong nonlinear phase distortions under certain conditions.

As in other cascaded $\chi^{(2)}$ processes, the sign of the phase mismatch determines the sign of the nonlinear phase shift. This in turn decides the sense of the distortion in the pump spectrum. As is shown in Fig. 17, when we assume that the second SHG channel is phase matched at 1545 nm, the simulated output pump spectrum shows a spectral dip on the longer-wavelength side, as opposed to the short-wavelength dip seen in Fig. 14.

We note that since there may be several waveguide modes, there is also the possibility of having more than one important additional cascaded $\chi^{(2)}$ process. Although the physical picture would become even more complicated, the results described above should still be relevant.

4. CONCLUSION

In conclusion, we have investigated high-power femtosecond SHG under large GVM conditions. It appears that a very strong NPM may contribute to a stronger-than-expected saturation of the SHG conversion efficiency at an approximately 60% level and to a distinct temporal and spectral distortion of the pump pulse. Our simulation results based on cascaded $\chi^{(2)}$ effects involving SHG to a second higher-order SH mode give a good qualitative and, in some cases, quantitative match to our experimental results, especially in light of the uncertainties in our model.

We believe we may have observed an interesting case of the interaction between a phase-matched SHG process and a second phase-mismatched SHG process, which results in a cascaded $\chi^{(2)}$ process, significantly changing the SHG yield. Such phenomena have not been reported previously to our knowledge and may have interesting scientific and practical significance. One of the most attractive features of QPM devices is the potential to permit one to engineer the nonlinearities. Our studies suggest that, for some applications, simultaneously controlling several waveguide modes may be necessary. This could become both a challenge and an opportunity to realize nonlinear optical waveguide devices with novel functionalities.

ACKNOWLEDGMENTS

The work at Purdue University was supported by the National Science Foundation under grant 9900369-ECS. The work at Stanford University was supported by the Defense Advanced Research Projects Agency through the Optoelectronic Materials Center. The authors acknowledge helpful discussions with Gennady Imeshev.

Z. Zheng's e-mail address is zzheng4@lucent.com.

*Present address, Lucent Technologies, Holmdel, N.J. 07733-3030.

†Present address, Tellium Inc., Oceanport, N.J. 07757-0901.

REFERENCES

1. W. H. Glenn, "Second-harmonic generation by picosecond optical pulses," IEEE J. Quantum Electron. **QE-5**, 284–290 (1969).
2. S. A. Akhmanov, A. P. Sukhorukov, and A. S. Chirkin, "Nonstationary phenomena and space-time analogy in nonlinear optics," Sov. Phys. JETP **28**, 748–757 (1969).
3. A. M. Weiner, A. M. Kan'an, and D. E. Leaird, "High-efficiency blue generation by frequency doubling of femtosecond pulses in a thick nonlinear crystal," Opt. Lett. **23**, 1441–1443 (1998).
4. Z. Zheng, A. M. Weiner, K. R. Parameswaran, M. H. Chou, and M. M. Fejer, "Low power spectral phase correlator using periodically poled $LiNbO_3$ waveguides," IEEE Photonics Technol. Lett. **13**, 376–378 (2001).
5. Z. Zheng and A. M. Weiner, "Spectral phase correlation of coded femtosecond pulses by second-harmonic generation in thick nonlinear crystals," Opt. Lett. **25**, 984–986 (2000).
6. L. E. Myers, R. C. Eckardt, M. M. Fejer, R. L. Byer, W. R. Bosenberg, and J. W. Pierce, "Quasi-phase-matched optical parametric oscillators in bulk periodically poled $LiNbO_3$," J. Opt. Soc. Am. B **12**, 2102–2115 (1995).
7. M. A. Arbore, M. M. Fejer, M. E. Fermann, A. Hariharan, A. Galvanauskas, and D. Harter, "Frequency doubling of femtosecond erbium-fiber soliton lasers in periodically poled lithium niobate," Opt. Lett. **22**, 13–15 (1997).
8. G. W. Ross, M. Pollnau, P. G. Smith, W. A. Clarkson, P. E. Britton, and D. C. Hanna, "Generation of high-power blue light in periodically poled $LiNbO_3$," Opt. Lett. **23**, 171–173 (1998).
9. M. A. Arbore, O. Marco, and M. M. Fejer, "Pulse compression during second-harmonic generation in aperiodic quasi-phase-matching gratings," Opt. Lett. **22**, 865–867 (1997).
10. G. Imeshev, A. Galvanauskas, D. Harter, M. A. Arbore, M. Proctor, and M. M. Fejer, "Engineerable femtosecond pulse shaping by second-harmonic generation with Fourier synthetic quasi-phase-matching gratings," Opt. Lett. **23**, 864–866 (1998).
11. G. Imeshev, M. A. Arbore, M. M. Fejer, A. Galvanauskas, M. Fermann, and D. Harter, "Ultrashort-pulse second-harmonic generation with longitudinally nonuniform quasi-phase-matching gratings: pulse compression and shaping," J. Opt. Soc. Am. B **17**, 304–318 (2000).
12. M. L. Bortz, S. J. Field, M. M. Fejer, D. W. Nam, R. G. Waarts, and D. F. Welch, "Noncritical quasi-phase-matched second harmonic generation in an annealed proton-exchanged $LiNbO_3$ waveguide," IEEE J. Quantum Electron. **30**, 2953–2960 (1994).
13. K. Kintaka, M. Fujimura, T. Suhara, and H. Nishihara, "High-efficiency $LiNbO_3$ waveguide second-harmonic generation devices with ferroelectric-domain-inverted gratings fabricated by applying voltage," J. Lightwave Technol. **14**, 462–468 (1996).
14. Y. Li, D. Guzun, and M. Xiao, "Quantum-noise measurements in high-efficiency single-pass second-harmonic generation with femtosecond pulses," Opt. Lett. **24**, 987–989 (1999).
15. J. A. Salehi, A. M. Weiner, and J. P. Heritage, "Coherent ultrashort light pulse code-division multiple access communication systems," J. Lightwave Technol. **8**, 478–491 (1990).
16. M. H. Chou, "Optical frequency mixers using three-wave mixing for optical fiber communications," Ph.D. Dissertation (Stanford University, Stanford, Calif., 1999).
17. O. Pfister, J. S. Wells, L. Hollberg, L. Zink, D. A. Van Baak, M. D. Levenson, and W. R. Bosenberg, "Continuous-wave

frequency tripling and quadrupling by simultaneous three-wave mixings in periodically poled crystals: application to a two-step 1.19–10.71-μm frequency bridge," Opt. Lett. **22**, 1211–1213 (1997).
18. R. Schiek, Y. Baek, and G. I. Stegeman, "Second-harmonic generation and cascaded nonlinearity in titanium-indiffused lithium niobate channel waveguides," J. Opt. Soc. Am. B **15**, 2255–2268 (1998).
19. L. Lepetit, G. Cheriaux, and M. Joffre, "Linear techniques of phase measurement by femtosecond spectral interferometry for applications in spectroscopy," J. Opt. Soc. Am. B **12**, 2467–2474 (1995).
20. R. DeSalvo, A. A. Said, D. J. Hagan, E. W. Van Stryland, and M. Sheik-Bahae, "Infrared to ultraviolet measurements of two-photon absorption and n_2 in wide bandgap solids," IEEE J. Quantum Electron. **32**, 1324–1333 (1996).
21. G. P. Agrawal, *Fiber-Optic Communication Systems*, 2nd ed. (Wiley, New York, 1997).
22. A. Yariv, "Coupled-mode theory for guided-wave optics," IEEE J. Quantum Electron. **QE-9**, 919–933 (1973).
23. G. P. Agrawal, *Nonlinear Fiber Optics*, 2nd ed. (Academic, San Diego, 1995).
24. C. R. Menyuk, "Stability of solitons in birefringent optical fibers. II Arbitrary amplitudes," J. Opt. Soc. Am. B **5**, 392–402 (1988).
25. M. H. Chou, I. Brener, M. M. Fejer, E. E. Chaban, and S. B. Christman, "1.5-μm-band wavelength conversion based on cascaded second-order nonlinearity in $LiNbO_3$ waveguides," IEEE Photonics Technol. Lett. **11**, 653–655 (1999).
26. M. Sheik-Bahae, D. C. Hutchings, D. J. Hagan, and E. W. Van Stryland, "Dispersion of bound electronic nonlinear refraction in solids," IEEE J. Quantum Electron. **27**, 1296–1309 (1991).
27. C. B. Clausen, O. Bang, and Y. S. Kivshar, "Spatial solitons and induced Kerr effects in quasi-phase-matched quadratic media," Phys. Rev. Lett. **78**, 4749–4752 (1997).
28. X. Liu, L. J. Qian, and F. Wise, "Effect of local phase-mismatch on frequency doubling of high-power femtosecond laser pulses under quasi-phase-matched conditions," Opt. Commun. **164**, 69–75 (1999).
29. C. R. Menyuk, R. Schiek, and L. Torner, "Solitary waves due to $\chi^{(2)}:\chi^{(2)}$ cascading," J. Opt. Soc. Am. B **11**, 2434–2443 (1994).
30. L. Torner, D. Mazilu, and D. Mihalache, "Walking solitons in quadratic nonlinear media," Phys. Rev. Lett. **77**, 2455–2458 (1996).
31. T. Iizuka and Y. S. Kivshar, "Optical gap solitons in nonresonant quadratic media," Phys. Rev. E **59**, 7148–7151 (1999).
32. S. Darmanyan, L. Crasovan, and F. Lederer, "Double-hump solitary waves in quadratically nonlinear media with loss and gain," Phys. Rev. E **61**, 3267–3269 (2000).
33. K. Koynov and S. Saltiel, "Nonlinear phase shift via multistep $\chi^{(2)}$ cascading," Opt. Commun. **152**, 96–100 (1998).
34. S. Saltiel, K. Koynov, Y. Deyanova, and Y. S. Kivshar, "Nonlinear phase shift resulting from two-color multistep cascading," J. Opt. Soc. Am. B **17**, 959–965 (2000).
35. S. Saltiel and Y. Deyanova, "Polarization switching as a result of cascading of two simultaneously phase matched quadratic processes," Opt. Lett. **24**, 1296–1298 (1999).
36. C. N. Ironside, J. S. Aitchison, and J. M. Arnold, "An all-optical switch employing the cascaded second-order nonlinear effect," IEEE J. Quantum Electron. **29**, 2650–2654 (1993).
37. X. Liu, L. J. Qian, and F. Wise, "High-energy pulse compression by use of negative phase shifts produced by the cascade $\chi^{(2)}:\chi^{(2)}$ nonlinearity," Opt. Lett. **24**, 1777–1779 (1999).
38. L. Becouarn, E. Lallier, M. Brevignon, and J. Lehoux, "Cascaded second-harmonic and sum-frequency generation of a CO_2 laser by use of a single quasi-phase-matched GaAs crystal," Opt. Lett. **23**, 1508–1510 (1998).
39. A. Arie, G. Rosenman, V. Mahal, A. Skliar, M. Oron, M. Katz, and D. Eger, "Green and ultraviolet quasi-phase-matched second harmonic generation in bulk periodically-poled $KTiOPO_4$," Opt. Commun. **142**, 265–268 (1997).